Environmental Science & Technology

pubs.acs.org/est

Article

Method of H_2 Transfer Is Vital for Catalytic Hydrodefluorination of Perfluorooctanoic Acid (PFOA)

Min Long, Yu Chen, Thomas P. Senftle, Welman Elias, Kimberly Heck, Chen Zhou,* Michael S. Wong, and Bruce E. Rittmann

Cite This: *Environ. Sci. Technol.* 2024, 58, 1390−1398

Read Online

ACCESS | Metrics & More | Article Recommendations | Supporting Information

ABSTRACT: The efficient transfer of H_2 plays a critical role in catalytic hydrogenation, particularly for the removal of recalcitrant contaminants from water. One of the most persistent contaminants, perfluorooctanoic acid (PFOA), was used to investigate how the method of H_2 transfer affected the catalytic hydrodefluorination ability of elemental palladium nanoparticles (Pd^0NPs). Pd^0NPs were synthesized through an in situ autocatalytic reduction of Pd^{2+} driven by H_2 from the membrane. The Pd^0 nanoparticles were directly deposited onto the membrane fibers to form the catalyst film. Direct delivery of H_2 to Pd^0NPs through the walls of nonporous gas transfer membranes enhanced the hydrodefluorination of PFOA, compared to delivering H_2 through the headspace. A higher H_2 lumen pressure (20 vs 5 psig) also significantly increased the defluorination rate, although 5 psig H_2 flux was sufficient for full reductive defluorination of PFOA. Calculations made using density functional theory (DFT) suggest that subsurface hydrogen delivered directly from the membrane increases and accelerates hydrodefluorination by creating a higher coverage of reactive hydrogen species on the Pd^0NP catalyst compared to H_2 delivery through the headspace. This study documents the crucial role of the H_2 transfer method in the catalytic hydrogenation of PFOA and provides mechanistic insights into how membrane delivery accelerates hydrodefluorination.

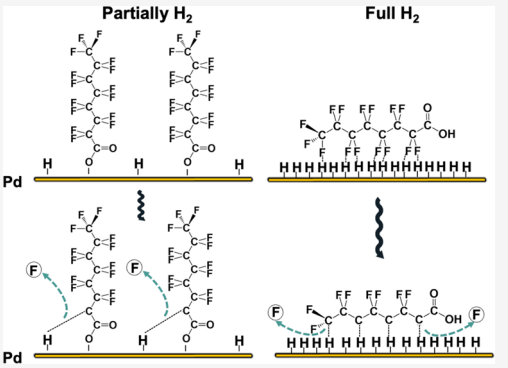

KEYWORDS: *hydrodefluorination, H_2 supply, Pd^0NPs, perfluorooctanoic acid (PFOA), activated hydrogen atoms (H*)*

INTRODUCTION

Catalytic hydrogenation, one of the most important processes in synthetic chemistry, involves the addition of molecular hydrogen (H_2) to unsaturated substrates, resulting in the formation of saturated products.[1] This versatile methodology has been extensively employed in the synthesis of pharmaceuticals, agrochemicals, and specialty chemicals.[2] Moreover, catalytic hydrogenation plays a pivotal role in environmental applications, such as the removal of recalcitrant contaminants, including halogenated (e.g., chlorophenols,[3] trichloroacetic acid,[4] and trichloroethane[5]) and nitrated (e.g., explosives such as TNT, PETN, and hexogen/RDX[6]) organic compounds.

H_2 plays a crucial role in catalytic hydrogenation by serving as a carrier of hydrogen atoms and their reducing equivalents.[7] H_2-induced hydrogenation involving metal catalysts occurs when both reactants (the oxidized contaminant and H_2) first adsorb on the catalyst surface.[8] For classical gas-phase hydrogenation, H_2 dissociates rapidly to become activated-H atoms on the catalyst's exterior surface, creating an equilibrium between gaseous molecular H_2 and surface-bound hydrogen atoms (H^*_{ads}).[9] H^*_{ads} atoms can migrate into the subsurface region within the catalyst's lattice, forming subsurface hydrogen species (H^*_{sub})[10] that often exhibit enhanced hydrogenation rates during heterogenous catalysis.[11−14]

In the gas phase, the initial formation of H^*_{ads} from H_2 and its subsequent subsurface intercalation in the Pd lattice occur rapidly.[15] The situation differs when the hydrogenation reactions occur in an aqueous solution, such as when treating halogenated water pollutants. The low water solubility of H_2 (0.016 g of H_2/kg of water at 20 °C) and the consequent slow rates of H_2 transfer from the gas phase to the bulk liquid and then to the catalyst surface (indirect H_2 transfer) significantly slow catalytic hydrogenation.[16] Conventional methods of delivering H_2 through bubbling and/or with a high-pressure headspace waste H_2 and can create a combustible atmosphere due to off-gassing. Depositing catalysts on nonporous hollow-fiber membranes provides precise bubble-free delivery of H_2 to the catalyst, which overcomes inefficient H_2 transfer due to low H_2 solubility and H_2 off-gassing that could create a combustion hazard.[17] The counterdirectional diffusion of H_2 and the oxidized contaminant makes the rate of H_2 delivery self-

Received: September 16, 2023
Revised: December 17, 2023
Accepted: December 20, 2023
Published: January 2, 2024

controlled. Furthermore, the delivery of H_2 to the base of the catalyst layer should promote the formation of reactive subsurface H^*_{sub} species while also eliminating the mass transfer limitation from the need to dissolve H_2 in the bulk liquid.[20]

Our previous research reported that catalytic activities in hydrogenation of recalcitrant oxidized contaminants, including trichloroethene and trichlorofluoromethane,[18] were significantly enhanced (10^2–10^4 times higher) when H_2 was delivered bubble-free to the catalysts (mostly zerovalent palladium nanoparticles (Pd^0NP)) deposited directly on the nonporous gas-transfer membranes. Herein, we study the underlying mechanisms by focusing on one of the most recalcitrant halogenated contaminants, perfluorooctanoic acid (PFOA, $C_7F_{15}COOH$).[19] We compare the performances of different H_2-transfer approaches for complete or partial PFOA hydrodefluorination catalyzed by Pd^0NP[20]

$$C_7F_{15}COOH + nH_2 \rightarrow C_7H_nF_{15-n}COOH + nH^+ + nF^- \quad (1 \le n \le 15) \quad (1)$$

In particular, we study the catalytic activity for hydrodefluorination of 10-μM PFOA, which is a level relevant to certain wastewaters and contaminated groundwaters.[21] The observation of much faster kinetics with direct membrane delivery supports the hypothesis that direct H_2 transfer from the membrane to the catalyst increases the population of surface H^*_{ads} and subsurface H^*_{sub}, which is the more active form of hydrogen[11,14,22] and which accelerates PFOA hydrodefluorination. To support this explanation, we used DFT calculations to examine how H* coverage affects PFOA adsorption and the differences in reactivity of H* atoms originating from the subsurface versus the surface during PFOA hydrodefluorination.

MATERIALS AND METHODS

Bench-Scale MCfR Setup. The configuration of the bench-scale membrane catalyst film reactor (MCfR), shown in Figure S1, was similar to that in our previous work.[20] The MCfR consisted of a 30 cm glass tube connected to a recirculation pump (Masterflex) giving a recirculation rate of 150 mL/min to mix the liquid contents thoroughly. The MCfR contained 120 hollow-fiber membranes (monolayer polypropylene; Teijin, Ltd., Japan) with an outer diameter of 200 μm, an inner diameter of 100 μm, and a wall thickness of 50 μm. Hydrogen gas (H_2) was provided to both ends of the bundle via a pressure regulator that controlled the H_2 pressure and H_2 delivery capacity.

Synthesis of Pd^0NP Catalysts. We prepared a Pd^{2+} precursor solution by dissolving 5 mM sodium tetrachloropalladate (Na_2PdCl_4) in deionized (DI) water, which gave a Pd loading of 0.9 g/m^2, which was the best loading in our previous PFOA study.[20] After filling the MCfR with the solution, the MCfR was kept in batch mode for 24 h until the liquid phase contained no more than 1% of the original Pd^{2+}. Pd^{2+} was autocatalytically reduced by H_2 to Pd^0 and deposited on the membrane, which was the source of H_2. By measuring the concentration of remaining Pd^{2+} in the liquid phase after 24 h, we calculated a total surface loading of 0.016 ± 0.002 g of Pd^0 deposited onto the membrane surface, giving a surface density of 0.9 ± 0.1 g/m^2. After the precursor liquid was drained from the MCfR, the MCfR was rinsed three times with DI water.

Batch Tests. Four freshly prepared MCfR reactors were operated under the following conditions: N_2 in the fiber lumen and headspace (no-H_2 control); H_2 in the headspace and N_2 in the fiber lumen; 5 psig (1.3 atm absolute) H_2 in the lumen; and 20 psig (2.3 atm absolute) H_2 in the lumen. The MCfRs were first purged with pure N_2 gas at 20 psig (2.3 atm absolute) for 15 min to eliminate O_2, and then, the PFOA stock solution (initial concentration = 10 μM, pH buffered at 4) was rapidly introduced (~10 s) using a feeding pump to begin each batch test. We collected liquid samples from the MCfR using 3 mL syringes and immediately filtered the sample through 0.22 μm PES membrane filters (NEST Scientific) to eliminate any solids for the subsequent analyses. Figure S2 shows that filtering did not result in any loss of PFOA.[23] The initial pH was buffered by adding 1.5 mM phosphate buffer, which maintained the pH and did not affect reactivity.

After a reaction was completed, we immersed the whole fibers into 40 mL of methanol for 7 days to extract PFOA from the Pd^0NP surface in order to quantify the total PFOA amount on the Pd^0NPs' surface. In the no-H_2 control (no hydrodefluorination), we achieved an average recovery of 97% of PFOA using methanol extraction. PFOA was measured after the methanol extraction.

Nanoparticle Collection and Solid-State Characterization. After the batch tests, we cut several pieces of the membrane from the MCfRs and prepared these samples according to our established procedure for solid-state analyses.[24] We examined the fibers using JEM-ARM200F scanning transmission electron microscopy (STEM), Krator Axis Supra X-ray photoelectron spectroscopy for valent analysis (XPS), and Malvern PANalytical Aeris X-ray powder diffraction (XRD).

Analyses of Liquid Samples and PFOA Adsorption Calculations. We utilized an ion chromatograph (IC-930, Metrohm) to analyze F^- and an Agilent 1290 UPLC coupled to a 6490 triple quadrupole mass spectrometer system (QQQ-MS) to measure PFOA based on the EPA Method 537.1.[20] Detailed analysis methods are summarized in Section 1 of the SI.

PFOA removed through defluorination was computed as the difference between the initial mass of PFOA and the sum of the masses in the liquid and on the surface. This computation is based on our understanding that PFOA retained on the Pd^0NP surface was present on sites of nondefluorinative adsorption, while the PFOA initially adsorbed to defluorinative sites had been defluorinated and removed. The proportions of nondefluorinative adsorption and defluorinative adsorption were calculated from

$$\text{nondefluorinative adsorption proportion} = \frac{\text{PFOA on the Pd}^0\text{NPs surface}}{\text{initial PFOA}} \quad (2)$$

$$\text{defluorinative adsorption proportion} = \frac{\text{PFOA defluorinated}}{\text{initial PFOA}} \quad (3)$$

Detailed calculations of the H_2-delivery capacity from the lumen and the PFOA flux are summarized in Section 2 in the SI.

The odds ratios for the peak area of the intermediate products were computed from

https://doi.org/10.1021/acs.est.3c07650
Environ. Sci. Technol. 2024, 58, 1390−1398

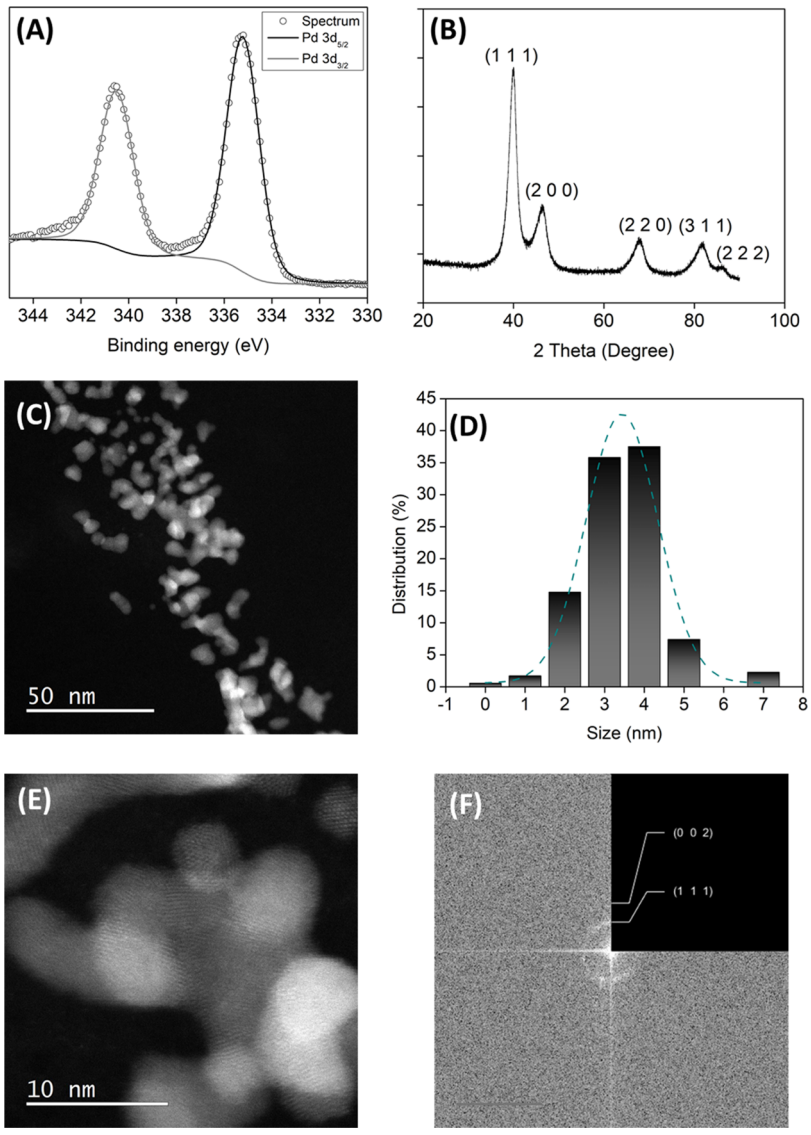

Figure 1. (A) XPS spectra of a Pd^0 fiber. (B) XRD spectra of a Pd^0 fiber. (C, E) TEM images of the cross-section of a Pd^0 fiber. (D) Size distribution of the nanoparticles of (C). (F) Diffraction patterns of Pd^0NPs from (E).

$$\ln \mathrm{OR} = \ln \frac{\varnothing_{\text{fiber 20 psig } H_2}}{\varnothing_{\text{fiber 5 psig } H_2}} \tag{4}$$

COMPUTATIONAL METHODS

The Vienna Ab initio Simulation Package[25] (VASP 5.4.4), in conjunction with the VASPsol implicit solvation model,[26] was applied to perform the DFT calculations. We used the same computational settings as reported in our previous work.[8]

To investigate how adsorption modes can be controlled by surface H* coverage, we computed the adsorption energy of the PFOA molecule ($\Delta E^{ads}_{Pd/PFOA}$) using eq 4

$$\Delta E^{ads}_{Pd/PFOA} = E_{Pd/PFOA} - E_{Pd} - E_{PFOA} \tag{5}$$

where $E_{Pd/PFOA}$ is the energy of PFOA adsorbed on the Pd surface, E_{Pd} is the energy of the Pd (111) slab at different H* coverages (i.e., 0 ML surface H*, 0.5 ML surface H*, 0.75 ML surface H*, 1 ML surface H*, as well as 1 ML surface H* and subsurface H*), and E_{PFOA} is the energy of the isolated PFOA molecule. The carboxylate headgroup forms Pd−O bonds with the Pd surface in perpendicular adsorption mode and only the tail chain group of PFOA interacts with the surface via van der Waals interactions in parallel adsorption mode.

We also calculated the reaction energy of the first PFOA hydrodefluorination step ($\Delta E_{H/F}$) at the α-position $-CF_2-$ (i.e., adjacent to $-COO^-$)[27] on the Pd^0 system in eq 6 (Figure 4A)

$$C_7F_{15}COO^- + \frac{1}{2}H_2 + H^* \rightarrow {}^* + C_7F_{14}HCOO^- + HF \tag{6}$$

using eq 7

$$\Delta E_{H/F} = E_* + E_{HF} + E_{C_7F_{14}HCOO^-} - E_{Pd-Rh-H^*} - \frac{1}{2}E_{H_2} - E_{C_7F_{15}COO^-} \tag{7}$$

where E_{HF}, E_{Pd-H_2}, and $E_{C_7F_{15}}COO^-$ represent the energy of the isolated HF, H_2, $C_7F_{14}HCOO^-$, and $C_7F_{15}COO^-$ molecules, respectively, E_{Pd-H^*} represents the energy of the Pd surface with 1 ML surface H* covering with or without the presence of

https://doi.org/10.1021/acs.est.3c07650
Environ. Sci. Technol. 2024, 58, 1390−1398

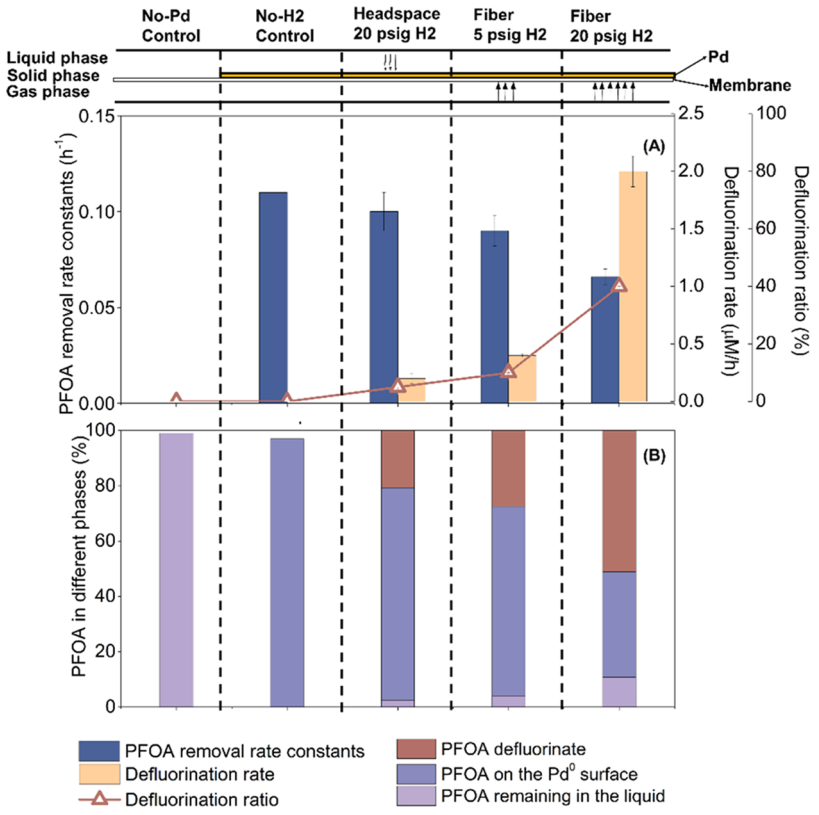

Figure 2. (A) PFOA removal rates, defluorination rate constants, and defluorination ratios for catalytic reductive defluorination of ~10 μM PFOA in the MCfR with Pd^{0}NPs at pH ~ 4 with 20 psig N_2, headspace H_2, 5 psig H_2, or 20 psig H_2. (B) Mass balances of PFOA concentration in different phases in the MCfR with Pd^{0}NPs at pH ~ 4 with 20 psig N_2, headspace H_2, 5 psig H_2, or 20 psig H_2. Controls have no Pd^{0}NPs and 20 psig H_2.

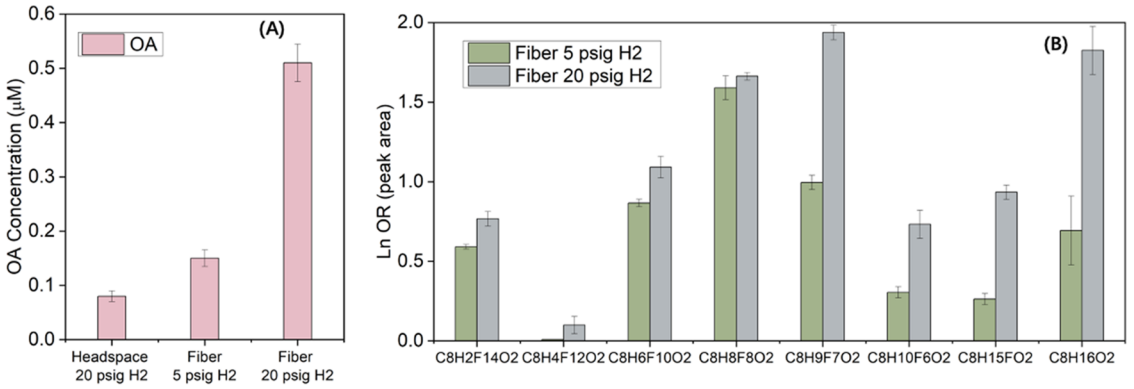

Figure 3. Odds ratios for the peak area of partially fluorinated products in Fiber 5 psig H_2 and Fiber 20 psig H_2 compared to Headspace 20 psig H_2.

subsurface H*, and E_* represents the corresponding surface with one surface H* removed.

RESULTS AND DISCUSSION

Characterization of Palladium on Membranes. Figure 1 presents the XPS, XRD, and STEM properties of a Pd film in the MCfR. The XPS analysis (Figure 1A) of the Pd film on the MCfR surface reveals the presence of fully reduced Pd^0, as evidenced by a single asymmetric peak in the Pd $3d_{5/2}$ energy at 335.3 eV and the Pd $3d_{3/2}$ energy at 340.5 eV.[28] The XRD analysis (Figure 1B) indicates the presence of Pd^0, with the characteristic (111) peak at 40.4 2θ degree. According to the STEM images of the Pd film (Figure 1C,E), Pd^{0}NPs were dispersed evenly and attached onto the membrane fibers as a continuous Pd^{0}NP film. The average size of the Pd^{0}NPs was 4.7 ± 0.7 nm based on 108 counts in Figure 1D, which is similar to those in the previously reported MCfR systems.[18] The diffraction patterns shown in Figure 1F indicate two planes of Pd^0, (111) and (200), which correspond to the XRD planes.

Batch Tests with Different H_2-Supply Methods. Figure 2 shows the results of catalytic hydrodefluorination of PFOA with Pd^{0}NPs using the same initial conditions: ~10 μM initial concentration of PFOA, 0.9 g/m^2 Pd^{0}NP loaded on the membranes, 22 °C, and pH 4. The figure presents the PFOA removal rate and degree of F^- release for the four H_2-supply methods, all with the Pd^{0}NPs deposited on the membranes: no-H_2 control, 20 psig H_2 in the headspace, and 5 psig H_2 or

https://doi.org/10.1021/acs.est.3c07650
Environ. Sci. Technol. 2024, 58, 1390−1398

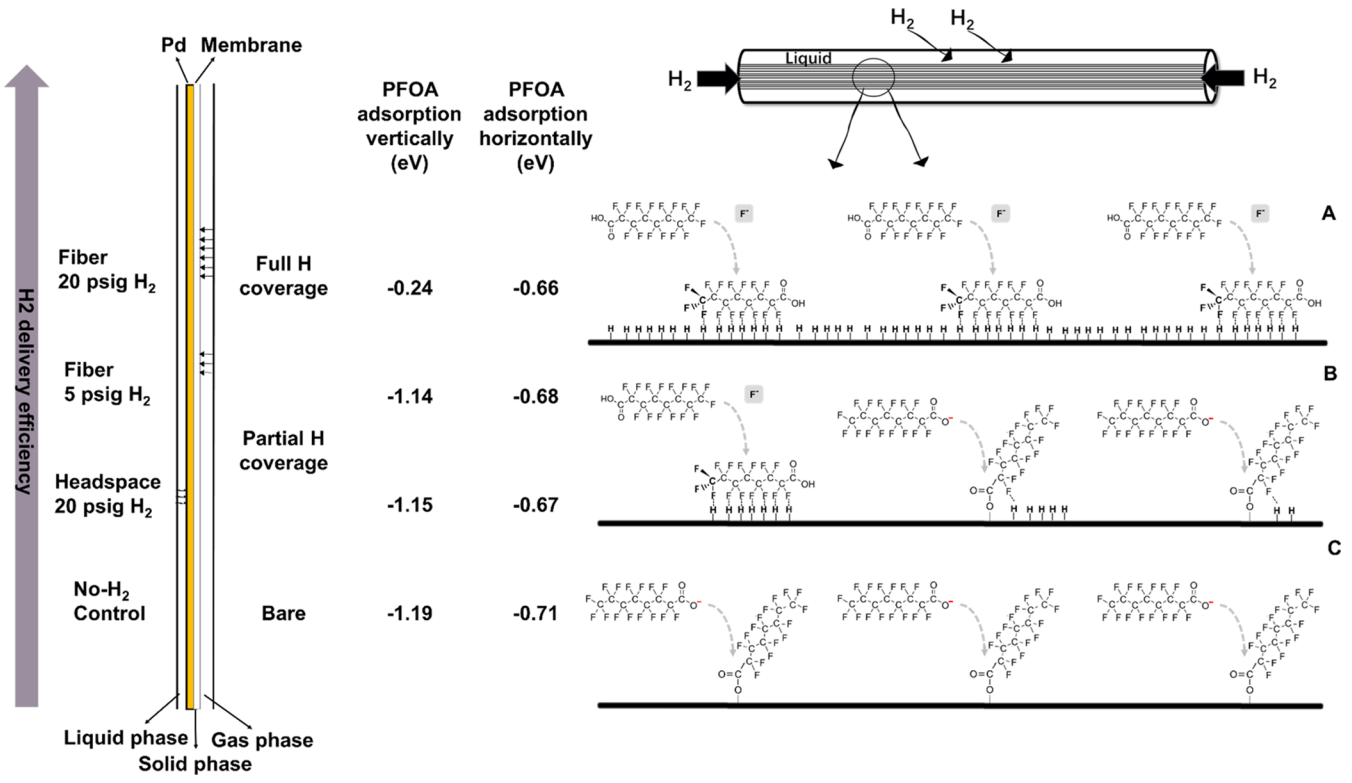

Figure 4. Adsorption configuration of $PFOA^-$ on the Pd^0 (111) surface in parallel and perpendicular adsorption modes at different H* surface coverage (bare, partially covered, and fully covered H*) along with the respective calculated adsorption energy.

20 psig H_2 supply through the membrane. Also shown is a no-Pd control. Figure 3 shows odds ratios for the peak area of partially fluorinated products in Fiber 5 psig H_2 and Fiber 20 psig H_2 compared to Headspace 20 psig H_2. The pH slightly decreased to 3.8 after the reaction.

Trade-Offs between Nondestructive and Hydrodefluorination Adsorptions on Pd^0NPs. In the absence of Pd^0NPs (the no-Pd control), 100% of the added PFOA remained in the liquid at the end of the batch test, indicating that neither adsorption nor defluorination occurred on the fibers. In the absence of H_2 and in the presence of N_2 (the no-H_2 control with Pd^0NPs), PFOA was depleted at a pseudo-first-order rate of 0.11 h^{-1}, but no F^- release was observed over 24 h. 160 μg of PFOA was extracted from the Pd^0NP surface, which means that 97% of the initial PFOA was retained via nondestructive adsorption on the Pd^0NP surface. In the presence of Pd^0NPs and H_2, PFOA removal occurred and F^- release was observed. Extraction of PFOA at the end of the experiment was significantly reduced, further confirming that the depletion of PFOA was substantially attributed to the destructive adsorption of PFOA on the Pd^0NP surface in the presence of H^*_{ads}. These phenomena verify that Pd^0NPs catalyzed PFOA defluorination only when H_2 was present.

Hydrodefluorination Kinetics and Degree Depending on the Gas-Transfer Approach. When 20 psig H_2 was supplied from the headspace, the rates of PFOA removal and F^- release were 0.1 h^{-1} and 0.2 μM/h, respectively (Figure 2A), and 77% of the initial PFOA was extracted with methanol. When the same 20 psig H_2 was supplied through the nonporous membrane, the rate of PFOA removal was 50% slower, but the rate of defluorination was 10-fold faster. Accordingly, only 37% of the initial PFOA was extracted from the Pd^0NP surface. When H_2 was supplied to the base of the Pd^0NP film (from the lumen of the hollow fibers via diffusion through the membrane wall), the bubble-free form of H_2 delivered through the membrane could be directly adsorbed by the Pd^0NPs deposited on the membrane surface, which eliminated the need for interphase mass transfer, enhanced the coverage of H* formation on the Pd^0NP surface,[15] and in turn increased the defluorination rate. Additional tests with a more facile nitrite reduction reaction (Section 4 and Table S2 of the SI) also indicate that H* was more abundant when H_2 was supplied from the nonporous membrane compared to delivery from the headspace. With H^*_{ads} blocking PFOA chemisorption (vide infra), increased coverage of H^*_{ads} also explains why the PFOA removal rate via adsorption was lower when 20 psig H_2 was delivered from the membrane compared to the headspace.

Hydrodefluorination Kinetics and Degree Varying with Different H_2 Fluxes. When 5 psig H_2 was supplied through the nonporous membrane, the rate constants for PFOA removal and F^- release were 0.09 h^{-1} and 0.4 μM/h, respectively, and 69% of the initial PFOA was extracted with methanol from the Pd^0NP surface. Compared to membrane delivery with a H_2 pressure of 20 psig, the rate of PFOA removal was 36% faster, but the rate of defluorination was fivefold slower. Accordingly, while 51% PFOA was removed through hydrodefluorination for 20 psig, it was only 27.5% for 5 psig. Thus, the lower H_2 pressure (5 vs 20 psig) dramatically decreased the defluorination rate, even though a lumen pressure of 5 psig H_2 had a H_2-supply capacity (57.5 e^- meq/m^2-day) much greater than the H_2 demand for full reductive defluorination of PFOA (0.86 e^- meq/m^2-day). This demonstrates that direct H_2 delivery via the membrane has another effect besides simply delivering enough of the reactive electron donor. This observation suggests that H_2 delivery

https://doi.org/10.1021/acs.est.3c07650
Environ. Sci. Technol. 2024, 58, 1390−1398

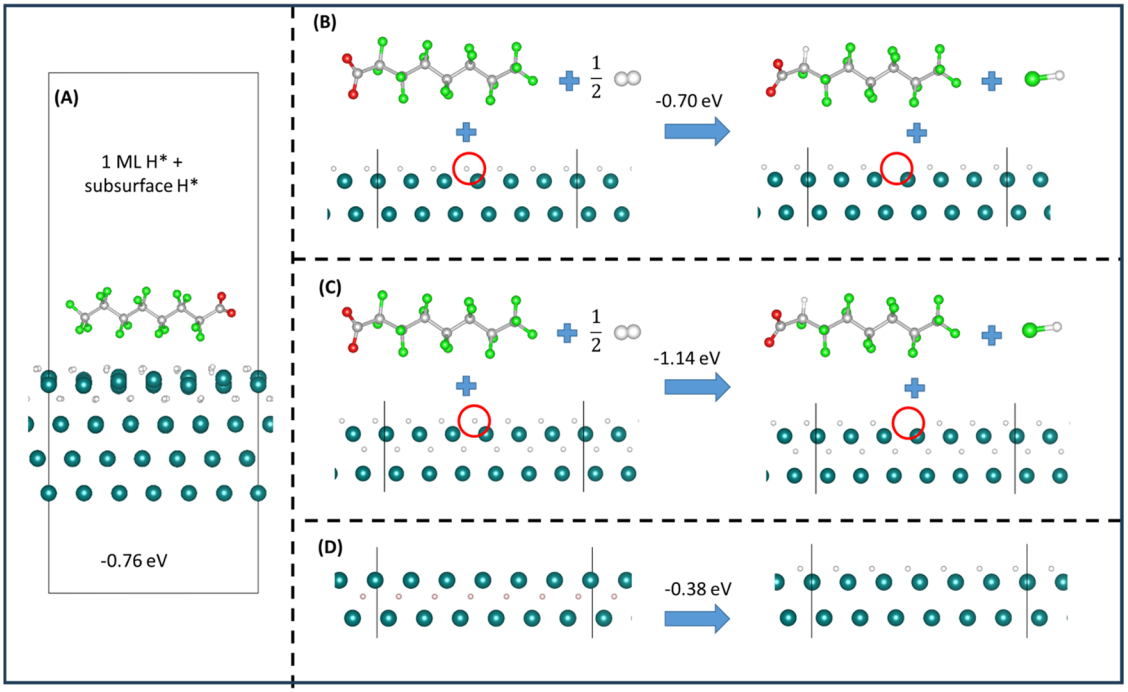

Figure 5. (A) Adsorption configuration of PFOA on the $Pd^0(111)$ surface in parallel mode with the subsurface H*. A schematic of the hydrodefluorination reaction of PFOA over a H*-covered $Pd^0(111)$ surface (B) without and (C) with subsurface H*: $C_7F_{15}COO^- + \frac{1}{2}H_2 + H^* \rightarrow {}^* + C_7F_{14}HCOO^- + HF$. The red circle highlights the reacting surface H* on the Pd^0 surface. (D) Resurfacing energy is −0.38 eV when subsurface H* migrates to surface H* in the Pd^0 system. The energy is computed on a per-H atom basis. Atom colors: green: F, gray: C, red: O, white: H, and dark green: Pd^0.

affects the H* coverage, which, in turn, impacts PFOA adsorption and defluorination rates.

As shown in Figure 3, the abundance of hydrodefluorination products, including partially and nonfluorinated products, increased after the reaction in water using 5 and 20 psig H_2 supplied through the membrane compared to 20 psig H_2 supplied indirectly from the headspace. Specifically, the concentration of the nonfluorinated product octanoic acid was less than 0.1 μM, and it was twofold higher with fiber delivery at 5 psig H_2 and fivefold higher with fiber delivery at 20 psig H_2. Moreover, the abundance of hydrodefluorination products with fiber delivery at 20 psig H_2 was greater than that with fiber delivery at 5 psig H_2, which is also consistent with the defluorination results.

In summary, H_2 delivered directly to the Pd^0NPs from nonporous membranes significantly increased the rate of defluorination over that of H_2 delivered through the headspace. As the H_2-delivery rate increased, the proportion of defluorinative adsorption increased: 0% (no-H_2 control), 21% (20 psig H_2 through the headspace), 28% (5 psig H_2 through the membrane), and 51% (20 psig H_2 through the membrane).

Mechanistic Insights into PFOA Adsorption and Defluorination with Varying H* Coverage. The experimental trends in the previous section demonstrate that the hydrogen coverage affected the PFOA adsorption and defluorination rates. We hypothesize that a high density of surface hydrogen atoms blocked the formation of direct chemical bonds between the PFOA carboxylate headgroup and the surface (i.e., chemisorption), which would explain the observed decrease in PFOA adsorption rates at higher H_2 pressures. At the same time, the more effective H_2 delivery through the membrane promoted defluorination because more H* species were available for the reaction. Figures 4 and 5 summarize our DFT calculations investigating how PFOA adsorption modes correlate with the H* surface/subsurface coverage and the related hydrodefluorination reaction energy.

As summarized in Figures 4 and S3, on a bare Pd(111) surface, deprotonated PFOA prefers to adsorb perpendicular to the surface through the formation of Pd−O bonds (i.e., chemisorption), where $\Delta E^{ads}_{Pd/PFOA} = -1.19$ eV. In contrast, PFOA adsorbs parallel to the surface on a fully H*-covered Pd(111) surface, where $\Delta E^{ads}_{Pd/PFOA} = -0.66$ eV. Adsorbed H* atoms block the formation of strong Pd−O bonds and prevent the carboxylate headgroup of PFOA from directly bonding to the surface, corroborating the experimental observation that PFOA adsorption is slower at higher H_2 pressure. We found that a Pd^0NP surface with partial H* coverage at 0.5 or 0.75 of a hydrogen monolayer (ML), where 1 ML corresponds to a surface with all sites occupied by H*, also leads to perpendicular PFOA adsorption through the carboxylate group: $\Delta E^{ads}_{Pd/PFOA} = -1.15$ eV at 0.5 ML and $\Delta E^{ads}_{Pd/PFOA} = -1.14$ eV at 0.75 ML. Thus, partial H* coverage only had a small effect on the PFOA-binding mode and strength because bare Pd sites still were available for PFOA chemisorption. These DFT computations demonstrate that when Pd sites do not have adsorbed H*, deprotonated PFOA tends to bind to those sites in a perpendicular orientation by forming strong Pd−O bonds. The defluorination rate is affected by the adsorption orientation of the PFOA molecule. We posit that parallelly bound PFOA more readily undergoes catalytic reduction by surface H* because of the proximity of the F atoms to the active H* sites on the surface. In contrast, a perpendicularly bound PFOA has a much greater separation

https://doi.org/10.1021/acs.est.3c07650
Environ. Sci. Technol. 2024, 58, 1390−1398

between H* on the surface and the C−F bonds in the molecule. This difference could explain the observed trade-off between adsorption rates and defluorination rates.

We also examined the hydrodefluorination reaction of PFOA over a H*-covered $Pd^0(111)$ surface with and without subsurface H*; the results are summarized in Figure 5. To understand how the presence of subsurface H* affected the hydrodefluorination of PFOA, we first computed the parallel adsorption energy of PFOA on the Pd surface with 1 ML (monolayer) surface H* and 1 ML subsurface H*. We found that subsurface H* did not substantially alter the PFOA adsorption strength (Figure 5A, $\Delta E^{ads}_{Pd/PFOA} = -0.76$ eV) compared to parallel adsorption on the surface with only 1 ML coverage of surface H* (Figure 4, $\Delta E^{ads}_{Pd/PFOA} = -0.66$ eV). Furthermore, we computed the hydrodefluorination reaction energy on the Pd^0 surface occurring via surface H* attack without ($\Delta E_{H/F} = -0.70$ eV) (Figure 5B) and with the presence of the subsurface H* ($\Delta E_{H/F} = -1.14$ eV) (Figure 5C) using eqs 6 and 7. The hydrodefluorination step was more thermodynamically favorable, by 0.44 eV, with subsurface H* present because subsurface H* destabilized the reacting surface H*.

H_2 that diffuses through the walls of the nonporous gas-transfer membrane creates subsurface H* species that emerge at the surface prior to attacking the C−F bond of the PFOA. As illustrated in Figure 5D, H* was more stable on the Pd surface compared to the subsurface by $\Delta E = -0.38$ eV. Thus, H* had a higher potential energy in the subsurface and naturally migrated toward the surface if vacant sites were available. When H* emerged at the surface, this potential energy was converted to kinetic energy that was either dissipated thermally or assisted in overcoming the C−F hydrodefluorination barrier. Since kinetic energy is quickly dissipated into surface vibrational modes on a picosecond time scale under equilibrium conditions, the kinetic energy can only be utilized if the system operates away from equilibrium.[13,29] For example, Ceyer et al. demonstrated the importance of subsurface H* in Ni(111) in methyl hydrogenation using a nonequilibrium experimental setup, in which the system was under high pressure to produce subsurface hydrogen and the surface hydrogen was removed with an atomic Xe beam.[14] We propose that the delivery of H_2 from the lumen in our experiments similarly created a large differential in the chemical potential of H_2, and the differential drove nonequilibrium H* from the subsurface to the surface, providing additional activity to overcome the C−F hydrodefluorination barrier.

Environmental Implications. This study revealed a critical factor that affects the hydrogenation of recalcitrant contaminants from water: Direct delivery of H_2 to Pd^0NPs through nonporous gas-transfer membrane walls enhanced the hydrodefluorination rate of PFOA compared to delivering H_2 through the headspace. Furthermore, a higher (20 psig) H_2 lumen pressure significantly increased defluorination rates, despite the fact that 5 psig H_2 had a delivery capacity sufficient to completely reductively defluorinate PFOA. DFT computations demonstrated that PFOA adsorption was highly sensitive to H* coverage and that PFOA defluorination was more energetically favorable when H* was migrated from the subsurface layers of the Pd^0 particles. These findings suggest that H_2 delivered to the reaction site by the gas-transfer membrane leads to higher H* coverage, affecting the PFOA adsorption and H* reactivity. Subsurface H* destabilizes surface H* atoms, thus increasing their reactivity toward PFOA. Furthermore, subsurface H* emerging at the surface may be more reactive than thermally equilibrated surface H* atoms, which also may contribute to the faster PFOA defluorination rates observed when H_2 was delivered through the membrane instead of through the headspace alone. The mechanisms are complicated, and we know that we are not yet able to interpret all aspects. Thus, we posit mechanisms that are directly based on our tests involving Pd loading and H_2 transfer as two key factors affecting the defluorination of PFOA. We will continue to search for deeper mechanistic insights in our future plan.

For recalcitrant contaminants such as PFOA, the direct transfer of H_2 to the Pd^0 catalyst enables hydrodefluorination by overcoming the challenges posed by the high C−F dissociation energy. The MCfR also is a promising approach for addressing other recalcitrant contaminants, e.g., trichloroethene and trichlorofluoromethane.[18] Furthermore, its potential for long-term operation makes it an especially promising solution for addressing real-world contamination. This study provides experimental and mechanistic insights into how membrane delivery accelerates hydrogenation, presenting an effective method for enhancing the catalytic destruction of recalcitrant contaminants.

■ ASSOCIATED CONTENT

Supporting Information

The Supporting Information is available free of charge at https://pubs.acs.org/doi/10.1021/acs.est.3c07650.

Chromatographic methods, calculation of the H_2-supply capacity and PFOA flux, detailed DFT methods, comparison of H coverage, schematic of the bench-scale MCfR system, PFOA concentrations before and after filtration, adsorption configuration of PFOA on the $Pd^0(111)$ surface, and F-verification (PDF)

■ AUTHOR INFORMATION

Corresponding Author

Chen Zhou − *Institute for the Environment and Health, Nanjing University, Suzhou 215163, China; State Key Laboratory of Pollution Control and Resource Reuse, School of the Environment, Nanjing University, Nanjing 210023, China;* orcid.org/0000-0002-8104-2848; Email: zhou_SCEB@asu.edu

Authors

Min Long − *State Key Laboratory of Pollution Control and Resource Reuse, College of Environmental Science and Engineering, Tongji University, Shanghai 200092, China;* orcid.org/0000-0001-5328-7787

Yu Chen − *Nanosystems Engineering Research Center for Nanotechnology-Enabled Water Treatment, Houston, Texas 77005, United States; Department of Chemical and Biomolecular Engineering, Rice University, Houston, Texas 77005, United States*

Thomas P. Senftle − *Nanosystems Engineering Research Center for Nanotechnology-Enabled Water Treatment, Houston, Texas 77005, United States; Department of Chemical and Biomolecular Engineering, Rice University, Houston, Texas 77005, United States;* orcid.org/0000-0002-5889-5009

https://doi.org/10.1021/acs.est.3c07650
Environ. Sci. Technol. 2024, 58, 1390−1398

Welman Elias − *Nanosystems Engineering Research Center for Nanotechnology-Enabled Water Treatment, Houston, Texas 77005, United States; Department of Chemical and Biomolecular Engineering, Rice University, Houston, Texas 77005, United States*

Kimberly Heck − *Nanosystems Engineering Research Center for Nanotechnology-Enabled Water Treatment, Houston, Texas 77005, United States; Department of Chemical and Biomolecular Engineering, Rice University, Houston, Texas 77005, United States*

Michael S. Wong − *Nanosystems Engineering Research Center for Nanotechnology-Enabled Water Treatment, Houston, Texas 77005, United States; Department of Chemical and Biomolecular Engineering, Rice University, Houston, Texas 77005, United States;* orcid.org/0000-0002-3652-3378

Bruce E. Rittmann − *Biodesign Swette Center for Environmental Biotechnology, Arizona State University, Tempe, Arizona 85287, United States;* orcid.org/0000-0002-3678-149X

Complete contact information is available at: https://pubs.acs.org/10.1021/acs.est.3c07650

Notes

The authors declare no competing financial interest.

■ ACKNOWLEDGMENTS

This work was partially supported by the National Science Foundation Engineering Research Center for Nanotechnology Enabled Water Treatment (EEC-1449500), the Strategic Environmental Research and Development Program (SERDP) (ER20-C1-1286), and Xylem Inc. (FP00019503). The authors acknowledge the use of facilities within the Eyring Materials Center and Mass Spectrometry at Arizona State University and thank the staff scientist involved in the data collection.

■ REFERENCES

(1) Yang, M.; Yu, J.; Zimina, A.; Sarma, B. B.; Pandit, L.; Grunwaldt, J. D.; Zhang, L.; Xu, H.; Sun, J. Probing the Nature of Zinc in Copper-Zinc-Zirconium Catalysts by Operando Spectroscopies for CO2 Hydrogenation to Methanol. *Angew. Chem., Int. Ed.* **2023**, *135* (7), No. e202216803.

(2) Fu, Q.; Luo, Y. Active sites of Pd-doped flat and stepped Cu (111) surfaces for H2 dissociation in heterogeneous catalytic hydrogenation. *ACS Catal.* **2013**, *3* (6), 1245−1252.

(3) Long, M.; Long, X.; Zheng, C.-W.; Luo, Y.-H.; Zhou, C.; Rittmann, B. E. Para-chlorophenol (4-CP) removal by a palladium-coated biofilm: coupling catalytic dechlorination and microbial mineralization via denitrification. *Environ. Sci. Technol.* **2021**, *55* (9), 6309−6319.

(4) Cai, Y.; Long, X.; Luo, Y.-H.; Zhou, C.; Rittmann, B. E. Stable dechlorination of Trichloroacetic Acid (TCAA) to acetic acid catalyzed by palladium nanoparticles deposited on H2-transfer membranes. *Water Res.* **2021**, *192*, No. 116841.

(5) Luo, Y.-H.; Zhou, C.; Bi, Y.; Long, X.; Wang, B.; Tang, Y.; Krajmalnik-Brown, R.; Rittmann, B. E. Long-term continuous co-reduction of 1, 1, 1-trichloroethane and trichloroethene over palladium nanoparticles spontaneously deposited on H2-transfer membranes. *Environ. Sci. Technol.* **2021**, *55* (3), 2057−2066.

(6) Zheng, C.-W.; Zhou, C.; Luo, Y.-H.; Long, M.; Long, X.; Zhou, D.; Bi, Y.; Yang, S.; Rittmann, B. E. Coremoval of Energetics and Oxyanions via the In Situ Coupling of Catalytic and Enzymatic Destructions: A Solution to Ammunition Wastewater Treatment. *Environ. Sci. Technol.* **2023**, *57* (1), 666−673.

(7) Federsel, C.; Jackstell, R.; Beller, M. State-of-the-art catalysts for hydrogenation of carbon dioxide. *Angew. Chem., Int. Ed.* **2010**, *49* (36), 6254−6257.

(8) Long, M.; Donoso, J.; Bhati, M.; Elias, W. C.; Heck, K. N.; Luo, Y.-H.; Lai, Y. S.; Gu, H.; Senftle, T. P.; Zhou, C. Adsorption and reductive defluorination of perfluorooctanoic acid over palladium nanoparticles. *Environ. Sci. Technol.* **2021**, *55* (21), 14836−14843.

(9) Conrad, H.; Ertl, G.; Latta, E. Adsorption of hydrogen on palladium single crystal surfaces. *Surf. Sci.* **1974**, *41* (2), 435−446.

(10) Landers, A. T.; Peng, H.; Koshy, D. M.; Lee, S. H.; Feaster, J. T.; Lin, J. C.; Beeman, J. W.; Higgins, D.; Yano, J.; Drisdell, W. S. Dynamics and Hysteresis of Hydrogen Intercalation and Deintercalation in Palladium Electrodes: A Multimodal In Situ X-ray Diffraction, Coulometry, and Computational Study. *Chem. Mater.* **2021**, *33* (15), 5872−5884.

(11) Ledentu, V.; Dong, W.; Sautet, P. Heterogeneous catalysis through subsurface sites. *J. Am. Chem. Soc.* **2000**, *122* (8), 1796−1801.

(12) Ashwell, A. P.; Lin, W.; Hofman, M. S.; Yang, Y.; Ratner, M. A.; Koel, B. E.; Schatz, G. C. Hydrogenation of CO to methanol on Ni (110) through subsurface hydrogen. *J. Am. Chem. Soc.* **2017**, *139* (48), 17582−17589.

(13) Henkelman, G.; Arnaldsson, A.; Jónsson, H. Theoretical calculations of CH 4 and H 2 associative desorption from Ni (111): could subsurface hydrogen play an important role? *J. Chem. Phys.* **2006**, *124* (4), No. 044706.

(14) Johnson, A.; Daley, S.; Utz, A.; Ceyer, S. The chemistry of bulk hydrogen: reaction of hydrogen embedded in nickel with adsorbed CH3. *Science* **1992**, *257* (5067), 223−225.

(15) Jewell, L. L.; Davis, B. H. Review of absorption and adsorption in the hydrogen−palladium system. *Appl. Catal., A* **2006**, *310*, 1−15.

(16) Zhao, F.; Zhang, R.; Chatterjee, M.; Ikushima, Y.; Arai, M. Hydrogenation of nitrobenzene with supported transition metal catalysts in supercritical carbon dioxide. *Adv. Synth. Catal.* **2004**, *346* (6), 661−668.

(17) Cheng, J.; Long, M.; Zhou, C.; Ilhan, Z.-E.; Calvo, D. C.; Rittmann, B. E. Long-Term Continuous Test of H2-Induced Denitrification Catalyzed by Palladium Nanoparticles in a Biofilm Matrix. *Environ. Sci. Technol.* **2023**, *57* (32), 11948−11957.

(18) Zhou, D.; Luo, Y.-H.; Zheng, C.-W.; Long, M.; Long, X.; Bi, Y.; Zheng, X.; Zhou, C.; Rittmann, B. E. H2-Based Membrane Catalyst-Film Reactor (H2-MCfR) Loaded with Palladium for Removing Oxidized Contaminants in Water. *Environ. Sci. Technol.* **2021**, *55* (10), 7082−7093.

(19) Gaines, L. G. Historical and current usage of per-and polyfluoroalkyl substances (PFAS): A literature review. *Am. J. Ind. Med.* **2023**, *66* (5), 353−378.

(20) Long, M.; Elias, W. C.; Heck, K. N.; Luo, Y.-H.; Lai, Y. S.; Jin, Y.; Gu, H.; Donoso, J.; Senftle, T. P.; Zhou, C. Hydrodefluorination of perfluorooctanoic acid in the H2-based membrane catalyst-film reactor with platinum group metal nanoparticles: pathways and optimal conditions. *Environ. Sci. Technol.* **2021**, *55* (24), 16699−16707.

(21) Rattanaoudom, R.; Visvanathan, C.; Boontanon, S. K. Removal of concentrated PFOS and PFOA in synthetic industrial wastewater by powder activated carbon and hydrotalcite. *J. Water Sustainability* **2012**, *2* (4), 245−258.

(22) Wang, W.; He, Y. H Resurface and Hot H Promoted H2 Recombination on Ni (111): Effects of Arrangement, Surface Coverage, and Lattice Motion. *J. Phys. Chem. C* **2021**, *125* (12), 6650−6659.

(23) Sörengård, M.; Franke, V.; Tröger, R.; Ahrens, L. Losses of poly-and perfluoroalkyl substances to syringe filter materials. *J. Chromatogr. A* **2020**, *1609*, No. 460430.

(24) Zhou, C.; Wang, Z.; Ontiveros-Valencia, A.; Long, M.; Lai, C.-y.; Zhao, H.-p.; Xia, S.; Rittmann, B. E. Coupling of Pd nanoparticles and denitrifying biofilm promotes H2-based nitrate removal with greater selectivity towards N2. *Appl. Catal., B* **2017**, *206*, 461−470.

(25) Kresse, G.; Furthmüller, J. Efficient iterative schemes for ab initio total-energy calculations using a plane-wave basis set. *Phys. Rev. B* **1996**, *54* (16), No. 11169.
(26) Mathew, K.; Kolluru, V. C.; Mula, S.; Steinmann, S. N.; Hennig, R. G. Implicit self-consistent electrolyte model in plane-wave density-functional theory. *J. Chem. Phys.* **2019**, *151* (23), No. 234101.
(27) Bentel, M. J.; Yu, Y.; Xu, L.; Li, Z.; Wong, B. M.; Men, Y.; Liu, J. Defluorination of per-and polyfluoroalkyl substances (PFASs) with hydrated electrons: structural dependence and implications to PFAS remediation and management. *Environ. Sci. Technol.* **2019**, *53* (7), 3718−3728.
(28) Guo, S.; Heck, K.; Kasiraju, S.; Qian, H.; Zhao, Z.; Grabow, L. C.; Miller, J. T.; Wong, M. S. Insights into nitrate reduction over indium-decorated palladium nanoparticle catalysts. *ACS Catal.* **2018**, *8* (1), 503−515.
(29) Klamroth, T.; Saalfrank, P. Effect of substrate vibrations on the sticking of atoms at surfaces: A critical comparison of different propagation methods for the H/Cu (100) system. *J. Chem. Phys.* **2000**, *112* (23), 10571−10581.

https://doi.org/10.1021/acs.est.3c07650
Environ. Sci. Technol. 2024, 58, 1390−1398